Author manuscript, published in "International Journal of Optomechatronics 6 (2012) 1-16"
DOI : 10.1080/15599612.2012.663462

hal-00799099, version 1 - 12 Mar 2013

Toward fast calibration of the global drift in scanning electron microscopes with respect to time and magnification

Abed C. Malti (a), Sounkalo Dembélé *(a), Nadine Piat (a),

Claire Arnoult (b), Naresh Marturi (a)

(a) FEMTO-ST/AS2M,

UMR CNRS 6174/Université de Franche-Comté/ENSMM/UTBM.

24 rue Alain Savary, 25000 Besançon, France.

(b) CRP Henri Tudor/AMS,

Technoport Schlassgoart, BP 144 -66,

rue de Luxembourg 4002 Esch s/ Alzette, Luxembourg.

Abstract

It is a well-known fact that the scanning electron microscopic image acquisition is mainly affected by nonlinearities and instabilities of the column and probe-specimen interaction; in turn producing a shift in the image points with respect to many parameters, time, in particular . Even though this drift is comparatively less in modern SEMs, it is still an important factor to consider in most of the SEM based applications. In this paper, a simple and real-time method is proposed to estimate the global

*corresponding author: sounkalo.dembele@femto-st.fr

hal-00799099, version 1 - 12 Mar 2013

drift from a set of target images using image phase correlation and to model its evolution by using the recursive equations of time and magnification. Based on the developed model, it is opted to use a Kalman filter in real time for accurate estimation and removal of the drift from images. The developed method is tested using the images from a tungsten filament gun SEM (Jeol JSM 820) and a field effect gun SEM (FEI Quanta 200) and the derived results show the effectiveness of the developed algorithm and also demonstrates its ability to be used in robotics as well as in material characterization under SEM.

Scanning electron microscope, calibration, drift, principal differential analysis

Nomenclature

SEM	scanning electron microscope
RMS	root mean square
PDA	principal differential analysis
ODE	ordinary differential equation
PDE	partial differential equation
SISO	single input single output
w.r.t	with respect to
t, t_0, t_f	time, initial time, final time
T	sampling time for calibration image acquisition
g, g_0, g_{f1}, g_f	magnification, initial magnification, intermediate magnification, final magnification
$\mathbf{A}, \mathbf{F}$	state matrices
$\mathbf{C}, \mathbf{G}$	output matrices

hal-00799099, version 1 - 12 Mar 2013

1 Introduction

1.1 Related work

In general, SEM is a powerful imaging instrument based on the electron-matter interaction. Conventionally it is comprised of an electron gun (to produce a continuous beam of electrons) along with many apertures and coils in order to reduce the generated beam diameter, accelerate, deflect and focus the beam on the supplied scanning surface of a specimen. As a final step, the images are produced by detecting the emitted electrons using special electron detectors (figure 1). Since the commercialization of SEM in 1970s it has become an essential tool in the study of nanomaterials and micronano systems mainly because of its advantages in observation, analysis and manipulation (Marchman, 1997),(Kasaya et al., 2004), (Sutton et al., 2006), (Sievers and Fatikow, 2006), (Jaehnisch and Fatikow, 2007), (Charlot et al., 2008), (Kratochvil et al., 2009), (Tosello et al., 2010), (Arnoult et al., 2010).

However, SEM image acquisition is known to be affected over time, mainly because of the presence of nonlinearities and instabilities during the raster scanning a specimen surface by the electron beam. As a result there is a shift in the image points w.r.t their projection model which in turn decomposes into drift and distortion (Maune, 1976), (Mizuno et al., 1997), (Santo et al., 2002), (Sutton et al., 2006), (Charlot et al., 2008),(Vignon et al., 2001), (Sinram et al., 2002), (Cornille, 2005), (Mizuno et al., 1997) and (Sicignano et al., 2004). Most of their work addresses the calibration of the projection and the distortion, very little deal with the calibration of drift. According to (Cornille, 2005), (Sutton et al., 2006),(Sutton et al., 2007) the pixel drift is estimated by the disparity between pairs of points and is fitted by B-splines w.r.t time. This model is used to estimate the drift and to remove it, in real time. The final accuracy is

hal-00799099, version 1 - 12 Mar 2013

very high that shows the relevance of the method and the fact it is convenient for metrology applications. This paper addresses the calibration of the drift in SEM images. It is focused on fast computation and removing of global drift in the images, instead of local drift. It also introduces the magnification of the SEM in the evolution of the drift and is convenient for robotic applications that require usually smooth change of magnification.

1.2 Contribution

The main contributions of this work are analysing and modelling the drift and developing a real-time algorithm to correct it. Generally the drift in a SEM is defined as the shift of pixels w.r.t to time, but many other constraints are also involved in the problem such as the physical magnification of the SEM, notably. As an initial approach the evolution of the drift is studied using image phase correlation w.r.t both time and magnification and is modelled by recursive equations of time and magnification. Many experiments with SEM require the dynamic change of magnification to fit with both the field-of-view and resolution. The developed model is such that it can deal with this change, accurately. The next contribution of the work is relative to the formalism adopted, Kalman filtering, which enables real time correction of the drift in images. The model of the drift is retrieved from a set of data obtained by phase correlation between the different pair of images, and is updated for every sampling step by taking into account the dynamic of the noise in the process.

1.3 Contents

Section 2 exposes the causes of the drift and the assumptions considered on which our current developments are based. Section 3 describes the way how the drift is estimated from a set of targeted image frames using phase correlation.

hal-00799099, version 1 - 12 Mar 2013

Section 4 addresses the learning stage of the approach developed: the estimation of the model of the drift with respect to time and magnification. Section 5 describes real time estimation and removal of the drift by using a Kalman filter. And finally, sections 6 and 7 presents respectively the results of the application of the approach to a tungsten filament gun SEM and a field effect gun SEM.

2 Preliminary assumptions

As mentioned earlier, the pixel drift is a result of instabilities present during the electron-specimen interaction and focusing inside the column. The main causes can be summarized as follows:

- Firstly, the image acquisition involves a lot of processes (probe beam emission, thining by magnetic lenses subjected to hysteresis, scanning by coils subjected to hysteresis, ...) that are not stable.
- Secondly, the specimen (possible defects or dust on the surface) is charged by electrons that causes the deflection of the electron beam, particularly for non conductive specimen. It affects also the emission of secondary electrons because of the low energy (about 50 eV). The consequence is a displacement of points in the images and thus, drift.
- Thirdly, thermal drift occurs since all components in the system are subject to temperature variations. These variations lead to expansion or contraction and to a deviation of the measured position.

One may see that too many phenomena intervene in the formation of the drift to make possible it description by theoretical equations. Empirical solutions are mandatory: the fitting of experimental drift by a function which define the model of the data and the use of the latter to estimate the drift in real time. The

hal-00799099, version 1 - 12 Mar 2013

empirical solution proposed in the paper is based on the assumptions described below.

1. SEM images are produced pixel by pixel following a rastering process. Rigorously speaking, the calibration of the drift requires the tracking of the pixels one by one: a drift function is associated to each. However, in this paper only the global drift between frames is considered that is easily assessed using cross correlation between pair of frames as exposed below.

2. The second assumption is to consider the drift as a function of two independent variables, the conventional time t, and the physical magnification of the SEM, g: $y(g,t), \hat{y}(g,t), t_0 \prec t \prec t_f, g_0 \prec g \prec g_f$. Indeed the drift is magnification dependant and many experiments require the change of magnification.

3 Experimental drift computation

Suppose $I(x,y)$ and $I'(x,y)$ be two pixels belonging to two image frames acquired at two different times. Suppose $I'(x,y)$ be $I(x,y)$ shifted by $(\delta_x, \delta_y)^\top$:

$$I'(x,y) = I(x - \delta_x, y - \delta_y) \tag{1}$$

Let their Fourier transforms be respectively $F(u,v)$ and $F'(u,v)$:

$$F'(x,y) = F(u,v) \exp -i2\pi(\frac{u}{M}\delta_x + \frac{v}{N}\delta_y) \tag{2}$$

The correlation between $F(u,v)$ and the conjugate of $F'(u,v)$ may be:

$$R(u,v) = \frac{F(u,v)\overline{F'(u,v)}}{|F(v,v)F'(u,v)|} = \exp -i2\pi(\frac{u}{M}\delta_x + \frac{v}{N}\delta_y) \tag{3}$$

hal-00799099, version 1 - 12 Mar 2013

with $M \times N$ the format of both images. $R(u,v)$ corresponds to the Fourier transform of the Dirac impulse shifted by $\delta = (\delta_x, \delta_y)^\top$, in the spatial domain: δ defines the drift between the pixels $I(x,y)$ and $I'(x,y)$. The computation of the inverse Fourier transform $H(\delta_x, \delta_y)$ of all the pixels of both images gives a kind of histogram with respect to the shift δ_x and δ_y: to each shift $(\delta_x, \delta_y)^\top)$ is associated the sum of Dirac impulses of the pair of pixels being shifted by that value. Finally the maximum of $H(\delta_x, \delta_y)$ enables to define the global $\Delta = (\Delta_x, \Delta_y)^\top$ drift between the second frame with respect to the former.

A calibration sample with random patterns, then convenient for drift measurement, is positioned upon the stage inside the chamber. It remains static and a set of images are acquired at time t from t_0 to t_f with a sampling step T and magnification g from g_0 to g_f with a sampling step G. The experimental drifts are obtained as described in algorithm 1.

```
for g = g_0 to g_f do
    timer = 0;
    t = t_0;
    for t = t_0 to t_f do
        Acquire an image frame of the calibration sample;
        timer = timer + T;
    end
    Compute the drift between the first image and the followings as
    described above;
    Change the area of scan to reduce the effect of the sample
    contaminations;
end
```

Algorithm 1: Algorithm for the computation of experimental drift

4 Modeling

Let consider the SEM as a SISO system with:

- an input $u(g,t)$ equals to zero,
- a state vector $\mathbf{x}(g,t)$,

hal-00799099, version 1 - 12 Mar 2013

- an output $y(g,t)$ corresponding to the drift.

Assume this system is described by the following recursive equations:

$$y(g,t-m)+a_{m-1}(g)y(g,t-(m-1))+\cdots+a_0(g)y(g,t)=0 \tag{4}$$

$$a_i(g-n)+b_{i,n-1}a_i(g-(n-1))+\cdots+b_{i,0}a_i(g)=0 \tag{5}$$

with $y(g,m-1)$ to $y(g,0)$ and $a_i(n-1)$ to $a_i(0)$ not null.

Above equations lead to the following state models:

$$\mathbf{x}(g,t)=\mathbf{A}(g)\mathbf{x}(g,t-1) \tag{6}$$

$$y(g,t)=\mathbf{C}\mathbf{x}(g,t) \tag{7}$$

$$\alpha_i(g)=\mathbf{F}_i\alpha(g-1) \tag{8}$$

$$a_i(g)=\mathbf{G}\alpha_i(g) \tag{9}$$

The states $\mathbf{x}$ and α are defined respectively as followed:

$$\mathbf{x}(t)=(y(t),y(t-1),\cdots,y(t-(m-1))^\top \tag{10}$$

$$\alpha_i(g)=(a_i(g),a_i(g-1),\cdots,a_i(g-(n-1))^\top \tag{11}$$

The matrices are defined as followed:

$$\mathbf{A}(g) = \begin{pmatrix} 0 & 1 & 0 & \cdots & 0 \\ 0 & 0 & 1 & \cdots & 0 \\ 0 & 0 & 0 & \cdots & 0 \\ 0 & 0 & 0 & \cdots & 1 \\ -a_0(g) & -a_1(g) & -a_2(g) & \cdots & -a_{m-1}(g) \end{pmatrix} \tag{12}$$

$$\mathbf{F}_i = \begin{pmatrix} 0 & 1 & 0 & \cdots & 0 \\ 0 & 0 & 1 & \cdots & 0 \\ 0 & 0 & 0 & \cdots & 0 \\ 0 & 0 & 0 & \cdots & 1 \\ -b_{i,0} & -b_{i,1} & -b_{i,2} & \cdots & -b_{i,n-1} \end{pmatrix} \tag{13}$$

$$\mathbf{C} = \begin{pmatrix} 1 & 0 & \cdots & 0 \end{pmatrix} \tag{14}$$

$$\mathbf{G} = \begin{pmatrix} 1 & 0 & \cdots & 0 \end{pmatrix} \tag{15}$$

The problem is the estimation of respectively the matrix $\mathbf{A}(g)$ (the weighting functions $a_i(g)$) and the matrices $\mathbf{F}_i$ (the weighting constants $b_{i,j}$) using the drift obtained from the calibration images. Many solutions may be found in the literature but we will adopt the PDA approach which consists in:

1. fitting the experimental data $z(s)$ by some combination of B-splines $\hat{z}(s)$,
2. minimizing the following quadratic function $J = N^{-1} \sum_i^{n_b} \left[\sum_{j=0} \rho_j \frac{d^j}{ds^j} \hat{z} \right]^2$, with ρ_j the weighting coefficients (i.e. $a_j(g)$ and $b_{i,j}$) and $\hat{z}$ corresponding to $\hat{y}$ and a_j.

The modeling algorithm may be that described in algorithm 2:

hal-00799099, version 1 - 12 Mar 2013

hal-00799099, version 1 - 12 Mar 2013

for $g = g_0$ **to** g_f **do**
  for $t = t_0$ **to** t_f **do**
    Estimate the coefficients $a_i(g)$ by means of PDA;
  end
  Estimate the coefficients $b_{i,j}$ by means of PDA;
end

Algorithm 2: Algorithm for modeling

5 Image frames correction

We suppose that the values of $\mathbf{x}(g,t)$ are corrupted by a zero mean noise $\omega(g,t)$ with the covariance $\mathbf{Q}(g)$. ω is supposed representing all the phenomena involved in the image formation and leading to noise in the image frames. The drift $y(g,t)$ is obtained from the computation of correlation and then may be considered as free of noise. As a consequence we will consider the usual noise of the output to be null. The equations of the system are then:

$$\mathbf{x}(g,t) = \mathbf{A}(g)\mathbf{x}(g,t-1) + \omega(g,t) \tag{16}$$

$$y(g,t) = \mathbf{C}\mathbf{x}(g,t) \tag{17}$$

These equations enable to write the Kalman filter time update equations (prediction),

$$\hat{\mathbf{x}}(g,t|t-1) = \mathbf{A}(g)\hat{\mathbf{x}}(g,t-1|t-1) \tag{18}$$

$$\mathbf{P}(g,t|t-1) = \mathbf{A}(g)\mathbf{P}(g,t-1|t-1)\mathbf{A}(g)^\top + \mathbf{Q}(g) \tag{19}$$

and the Kalman filter state update equations (correction),

$$K(g,t) = \mathbf{P}(g,t|t-1)\mathbf{C}^\top(\mathbf{C}(g)\mathbf{P}(g,t|t-1)\mathbf{C}(g)^\top)^{-1} \tag{20}$$

hal-00799099, version 1 - 12 Mar 2013

$$\hat{\mathbf{x}}(g,t|t) = \hat{\mathbf{x}}(g,t|t-1) + K(g,t)(y(g,t) - C(g)\hat{\mathbf{x}}(g,t|t-1)) \tag{21}$$

$$\mathbf{P}(g,t|t) = (\mathbf{I} - K(g,t)\mathbf{C}(g))\mathbf{P}(g,t|t-1) \tag{22}$$

$\mathbf{P}$ is the state error covariance.

Considering any image frame acquired at time t and magnification g, it drift may estimated as described above and then removed according to the algorithm 3.

while *true* **do**
  Acquire image frame at t and g;
  Predict the state according to the equation 18;
  Predict the state error covariance according to the equation 19;
  Compute the Kalman filter gain according to equation 20;
  Update the state according to equation 21;
  Update the state error according to equation 22;
  Extract the two components of the drift Δ_x and Δ_y;
  Replace every point $I(x,y)$ of the image frame by $I(x-\Delta_x, x-\Delta_y)$;
end

Algorithm 3: Algorithm for filtering and correction

Of course it is necessary to initialize the process before:

1. two images will be acquired at two different times and their drift will be used as initial data,
2. the state error covariance matrix will be null.

Finally the complete calibration procedure may be described by the flow chart of figure 2.

hal-00799099, version 1 - 12 Mar 2013

6 Application to a tungsten SEM

6.1 Experimental drift

The calibration method developed so far is applied onto a Jeol JSM 820 SEM (figure 1). It is equipped with a Tungsten filament that can support from 0.3 up to $30KV$ of acceleration voltage. During all the experiments the acquisition characteristics are: high vacuum, $15KV$, $20mm$ working distance, 512×512 pixels image format, $30s$ scanning time per image. The specimen is a gold-on-silicon specimen with the particle size up to 500 nm (figure 3).

A set of 55 images per magnification are acquired each 30 seconds. The magnification is tuned from $100\times$ until $30,000\times$ with a step of $500\times$. Some of these images are shown in figure 4 with an illustration of the cross-correlation resulting peaks between the first frame and the followings (figure 5).

The two components of the drift vector of all images across time and magnification are depicted in figures 6 and 7. The drift increases with time and magnification in a nonlinear way. It reaches $(20,90)^\top pixels$ after 20 min and at 30 $K\times$ magnification, which is a really high value. It indicates the impossibility to use that SEM without calibration for long time measurement experiment.

6.2 Correction

The PDA analysis exhibit a 2rd recursive for the time dependence and a 2nd recursive for the magnification dependence. The performance of the approach is evaluated through some validating image data. The obtained prediction error curves across time and scales are depicted in figures 8 and 9. Less than 1.5 pixel error in the x-axis and less than 1 pixel error in y-axis can be observed.

hal-00799099, version 1 - 12 Mar 2013

Also, 0.28 pixel of global RMS error in x-axis and 0.23 pixel of RMS error in y-axis can be observed.

The computation time is evaluated for four implementations, Matlab, C++, C++ with OpenMP (parallel programming package) and C, on a Intel dual core 2, 1 GB SDRAM (figure 10). These times are low enough to enable real time use of the approach since the acquisition speed of the SEM is usually weak to enable exploitable images.

7 Application to a FE SEM

7.1 Experimental drift

The calibration method is applied onto a Fei Quanta 200 which is equiped with a FEG of the type Schotky. The experimental conditions are: High vacuum, $15KV$, 3 Spot size, $10mm$ working distance, 1024×884 pixels per image, $27.8s$ scanning time per image. The specimen is a tin-on-carbon specimen with the particle size up to 60 nm (figure 11).

The two components of the drift vector of all images across time and magnification are depicted in figures 12 and 13.

As expected the results are comparatively better than the one from the tungsten SEM. It is mainly because of the high stability provided by the FE SEM.

8 Conclusion

Scanning electron microscopes, particularly those using tungsten filament, are affected by drift. The calibration (estimation and correction) of this phenomenon is an important issue if one want to use a SEM for measurement

hal-00799099, version 1 - 12 Mar 2013

like in material characterization (deformation measurement) or in visual servoing (sample handling). Some modern SEMs have improved the instabilities and nonlinearities of the images formation and then reduce the drift drastically. But these are few and most of SEMs still exhibits huge amount of drift and then requires the use of calibration method to remove the drift. This problem is investigated in the paper.

The developments are based on three main ideas:

- the estimation of the drift between a pair of images by means of phase correlation which gives accurate results,
- the acquisition of some reference images with respect to time and magnification and their use to estimate a model of the drift,
- the real time estimation of the drift using a Kalman filtering and it removing from images.

Their application to the analysis of two types of SEM shows their relevance: a tungsten filament SEM (Jeol JSM 820) exhibits more important values of the drift than a field effect gun SEM one (Fei Quanta 200) and in both cases the drift has been removed with accuracy, finally. The approach enables to overcome the limitation of state-of-the-art drift calibration methods to handle smooth variations of magnification scales.

But the experiments point out some limitations of the method which will be investigated deeper.

The resolution of the method will be improved by replacing the PDA approach by a more accurate parameters estimation method, and by estimating accurately the state error covariance from the images of the target specimen.

The work will be extended from global drift over a pair of images to the local drift of every pair of pixels. Indeed the material is not uniform and the drift is

hal-00799099, version 1 - 12 Mar 2013

specific to every pair.

Recent works with pressure controlled SEM suggest an existing influence of the pressure on the drift and the spatial distortion especially at very high magnifications (Arnoult et al., 2010). It is planned to introduce the pressure as another variable and to quantify its impact. Henceforth, it will be challenging to validate the approach with further experiments at very high magnification scales as enabled by FEG based SEMs.

ACKNOWLEDGEMENTS *This work is conducted with financial support from the project (BQR) dealing with the calibration of scanning electron microscope funded by Université de Franche Comté.*

The authors thank a lot Roland Salut from FEMTO-ST/MIMENTO, Andres Marina-Diaz master student at ENSMM and Aliyassin El Ayouch master student at Université de Franche Comté.

References

ARNOULT, C., C. SPERANDIO, A. LAACHACHI, D. RUCH, AND J. DI MARTINO (2010). *Methodology of composite polymers/metal interface characterization by adapted EDX profiling in a pressure controlled SEM*, CHAPTER MICROSCOPY: SCIENCE, TECHNOLOGY, APPLICATIONS AND EDUCATION, PP. 1211–1218. MICROSCOPY. BADAJOZ: FORMATEX RESEARCH CENTER.

CHARLOT, F., P. JONNARD, F. ROUSSEL, J. RUSTE, F. GRILLON, A. JADIN, C. MATTIEU, M. RIPOUX, R. PASSAS, G. THOLLET, F. BRISSET, A. MALCHERE, F. MANIGUET, D. B. ET C. GENDARME, A. CRISCI, J. POUCHOU, F. ROBAUT, T. BAUDIN, A. ETTER, J. CAZAUX, M. BETBEDER, P. HALLEGOT, J. LECHAIRE, D. DUPEYRE, J. CHAIX, J. MISSIAEN, R. CHIRON, G. AUVERT, P. DONNADIEU, AND F. DONATINI (2008). *Microscopie électronique á balayage et microanalyses.* PARIS: EDP SCIENCES.

hal-00799099, version 1 - 12 Mar 2013

Cornille, N. (2005). *Accurate 3D Shape and Displacement Measurement using a Scanning Electron Microscope.* Ph. D. thesis, Ecole des Mines d'Albi-Carmaux. Albi, France.

Jaehnisch, M. and S. Fatikow (2007). 3-d vision feedback for nanohandling monitoring in a scanning electron microscope. *International Journal of Optomechatronics 1*(1), 4–26.

Kasaya, T., H. Miyazaki, S. Saito, K. Koyano, T. Yamaura, and T. Sato (2004). Image-based autonomous micromanipulation system for arrangement of spheres in a scanning electron microscope. *Review of scientific instruments 75*(6), 2033–2042.

Kratochvil, B. E., L. Dong, and B. J. Nelson (2009). Real-time rigid-body visual tracking in a scanning electron microscope. *International Journal of Robotics Research 28*(4), 498–511.

Marchman, H. (1997). Scanning electron microscope matching and calibration for critical dimensional metrology. *Journal of Vacuum Science and Technology B 15*(6), 2155–2161.

Maune, D. F. (1976). Photogrammetric self-calibration of scanning electron microscopes. *Photogrammetric Engineering and Remote Sensing 42*(9), 335–357.

Mizuno, F., M. Shimizu, and K. Sasada (1997). Evaluation of the long-term stability of critical-dimension measurement scanning electron microscopes using a calibration standard. *Journal of Vacuum Science and Technology B 15*(6), 2177–2180.

Santo, I., M. Ataka, K. Takahashi, and N. Anazawa (2002). Calibration and long-term stability evaluation of photo mask cd-sem utilizing jqa standard. In *Proceedings of SPIE*, Volume 4889(1), pp. 328–335.

hal-00799099, version 1 - 12 Mar 2013

Sicignano, A., A. Nikitin, D. Yeremin, T. Goldburt, and B. Tracy (2004). A novel and robust method for the accurate magnification characterization and calibration of out-of-fab sem cluster tools. In *Proceedings of SPIE*, Volume 5375, pp. 1069–1080.

Sievers, T. and S. Fatikow (2006). Real-time object tracking for the robot-based nanohandling in a scanning electron microscope. *Journal of Micromechatronics 3*(3-4), 267–284.

Sinram, O., M. Ritter, S. Kleindiek, A. Schertel, H. Hohenberg, and J. Albertz (2002). Calibration of an sem using a nanopositioning tilting table and a microscopic calibration pyramid. In *International Symposium of Photogrammetry and Remote Sensing*, Volume 35 (5), pp. 210–216.

Sutton, M., N. Li, D. Garcia, N. Cornille, J. Orteu, S. McNeill, H. Schreier, X. Li, and A. Reynolds (2007). Scanning electron microscopy for quantitative small and large deformation measurements part ii: Experimental validation for magnifications from 200 to 10,000. *Experimental Mechanics 47*(6), 789–804.

Sutton, M. A., N. Li, D. Garcia, N. Cornille, J. J. Orteu, S. R. McNeill, H. W. Schreier, and X. Li (2006). Metrology in a scanning electron microscope: theoretical developments and experimental validation. *Measurement science and technology 17*(10), 2613–2622.

Tosello, G., H. Hansen, F. Marinello, and S. Gasparin (2010). Replication and dimensional quality control of industrial nanoscale surfaces using calibrated afm measurements and sem image processing. *CIRP Annals - Manufacturing technology 59*(1), 563–568.

Vignon, F., G. L. Besnerais, D. Boivin, J.-L. Pouchou, and L. Quan (2001). 3d reconstruction from scanning electron microscopy using stereovision and self-calibration. In *Physics in Signal and Image Processing*, Volume 1(1), pp. 129–134.

hal-00799099, version 1 - 12 Mar 2013

9 Figures

List of Figures

1 Tungsten SEM: view and composition. 20
2 Flow chart describing the complete calibration procedure proposed 21
3 Tungsten SEM: images of the gold-on-silicon calibration specimen at $10K\times$ (left) and $30K\times$ (right). 21
4 Tungsten SEM: some images of the gold-on-silicon calibration specimen at four different times and three different magnifications. 22
5 Tungsten SEM: the cross-correlation functions between the first image and the followings of figure 4: the bright points correspond to the maximum. 23
6 Tungsten SEM: the drift with respect to time and magnification along x-axis. 24
7 Tungsten SEM: the drift with respect to time and magnification along y-axis. 25
8 Tungsten SEM: the absolute error of drift with respect to time and magnification along x-axis. 26
9 Tungsten SEM: the absolute error of drift with respect to time and magnification along y-axis. 27
10 Tungsten SEM: the execution speed (in ms) of the correction for four implementations. 28
11 FE SEM: images of the tin-on-carbon calibration specimen at $1K\times$ (left) and $10K\times$ (right). 28
12 FE SEM: the drift with respect to time and magnification along x-axis. 29

13 FE SEM: the drift with respect to time and magnification along y-axis. 30

hal-00799099, version 1 - 12 Mar 2013

hal-00799099, version 1 - 12 Mar 2013

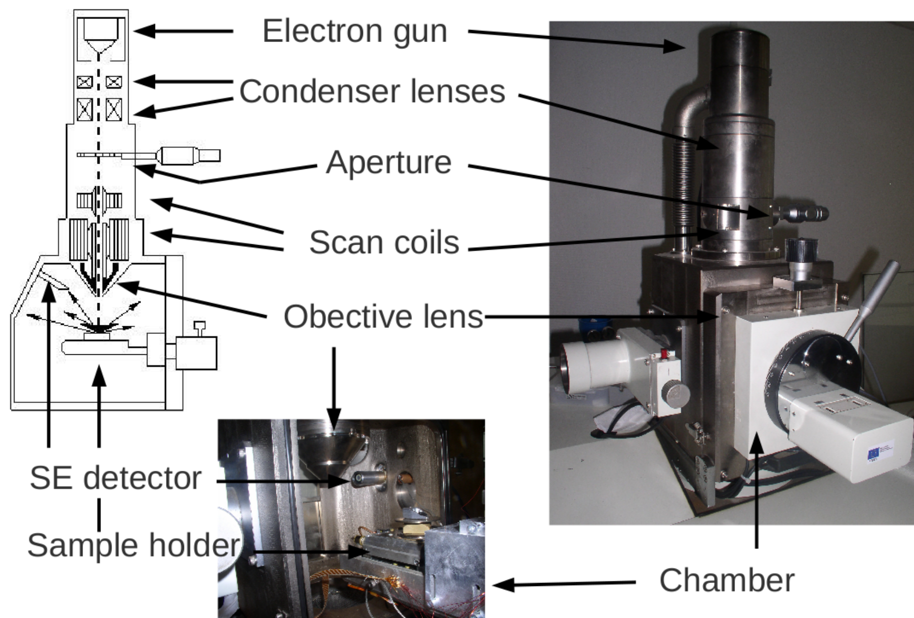

Figure 1: Tungsten SEM: view and composition.

hal-00799099, version 1 - 12 Mar 2013

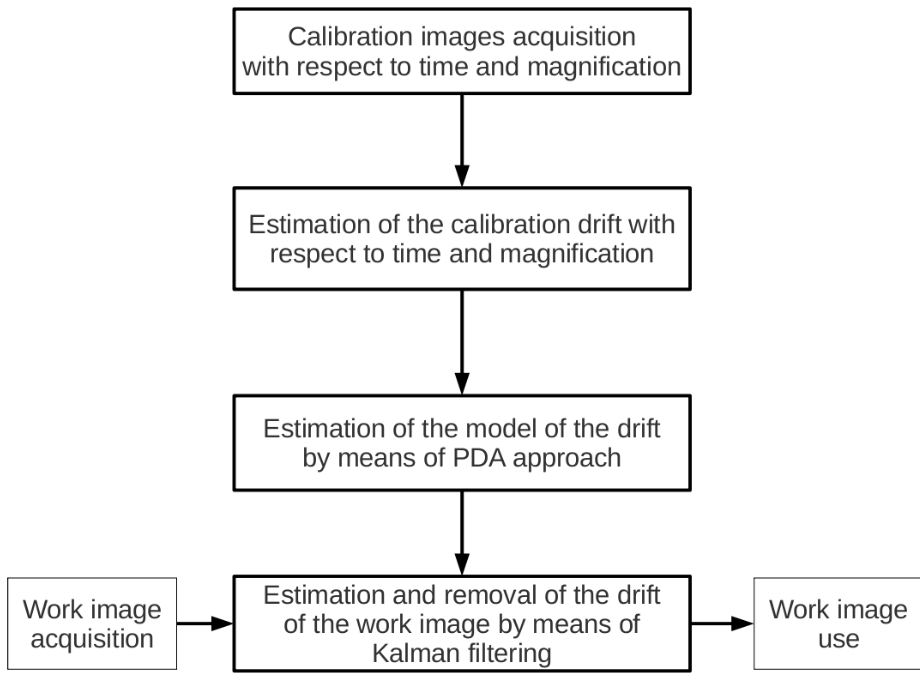

Figure 2: Flow chart describing the complete calibration procedure proposed

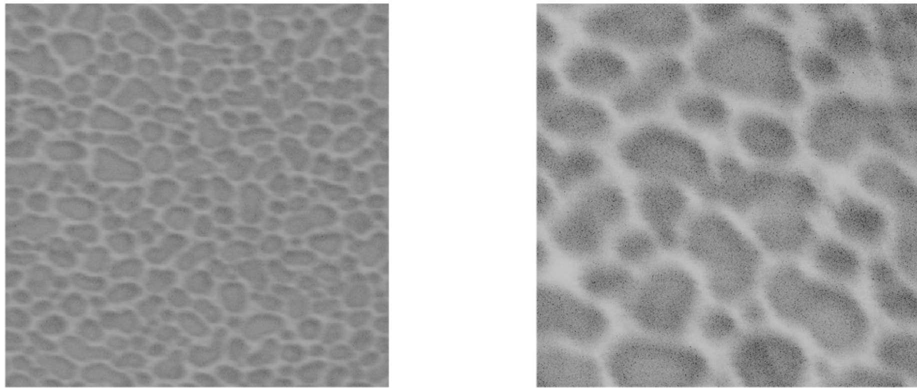

Figure 3: Tungsten SEM: images of the gold-on-silicon calibration specimen at $10K\times$ (left) and $30K\times$ (right).

hal-00799099, version 1 - 12 Mar 2013

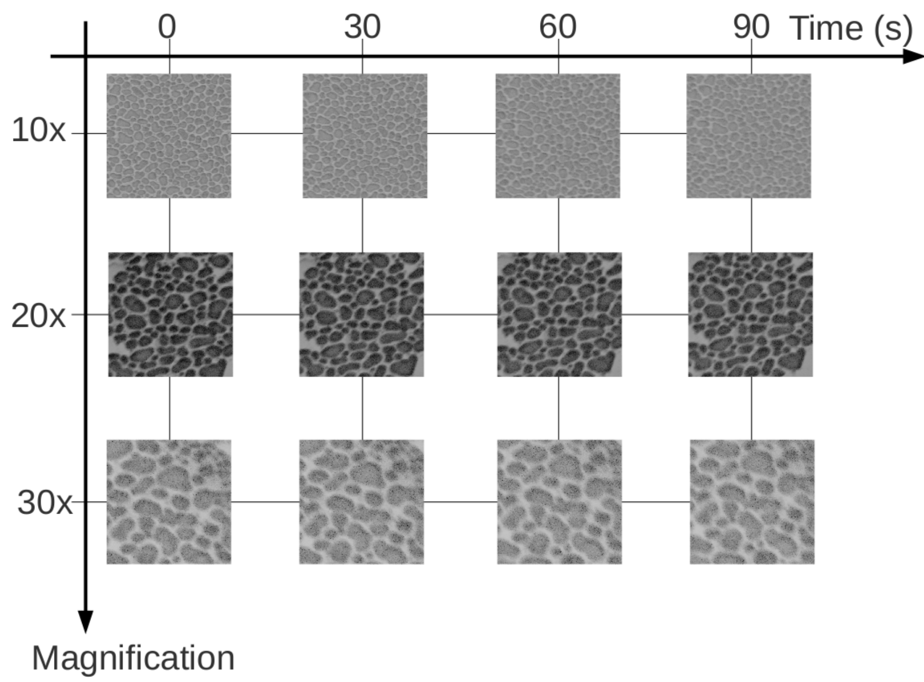

Figure 4: Tungsten SEM: some images of the gold-on-silicon calibration specimen at four different times and three different magnifications.

hal-00799099, version 1 - 12 Mar 2013

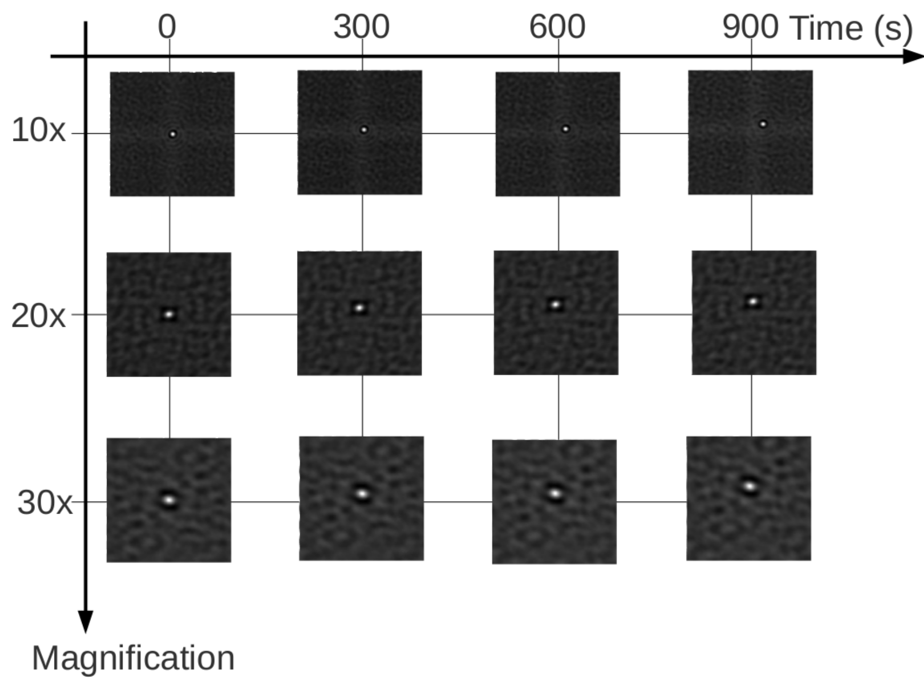

Figure 5: Tungsten SEM: the cross-correlation functions between the first image and the followings of figure 4: the bright points correspond to the maximum.

hal-00799099, version 1 - 12 Mar 2013

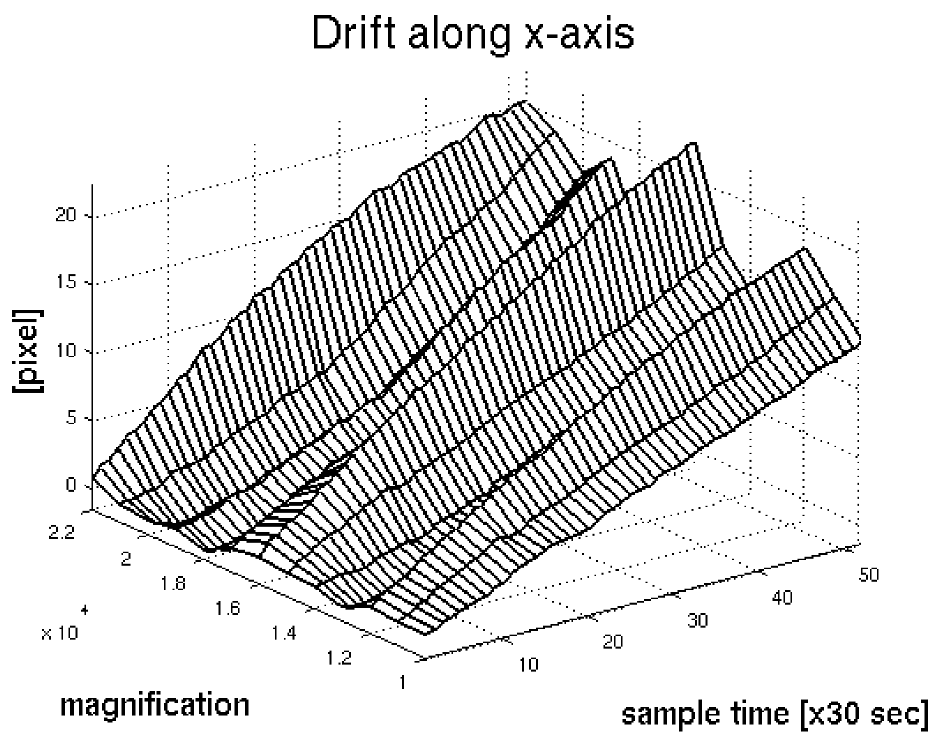

Figure 6: Tungsten SEM: the drift with respect to time and magnification along x-axis.

hal-00799099, version 1 - 12 Mar 2013

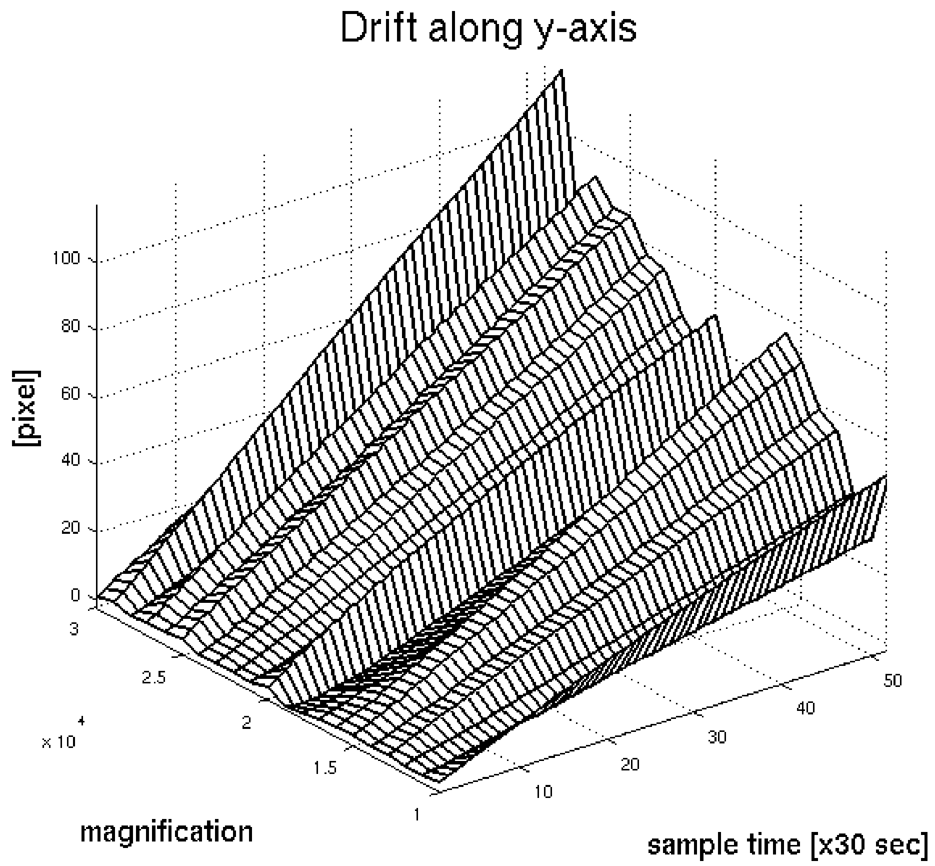

Figure 7: Tungsten SEM: the drift with respect to time and magnification along y-axis.

hal-00799099, version 1 - 12 Mar 2013

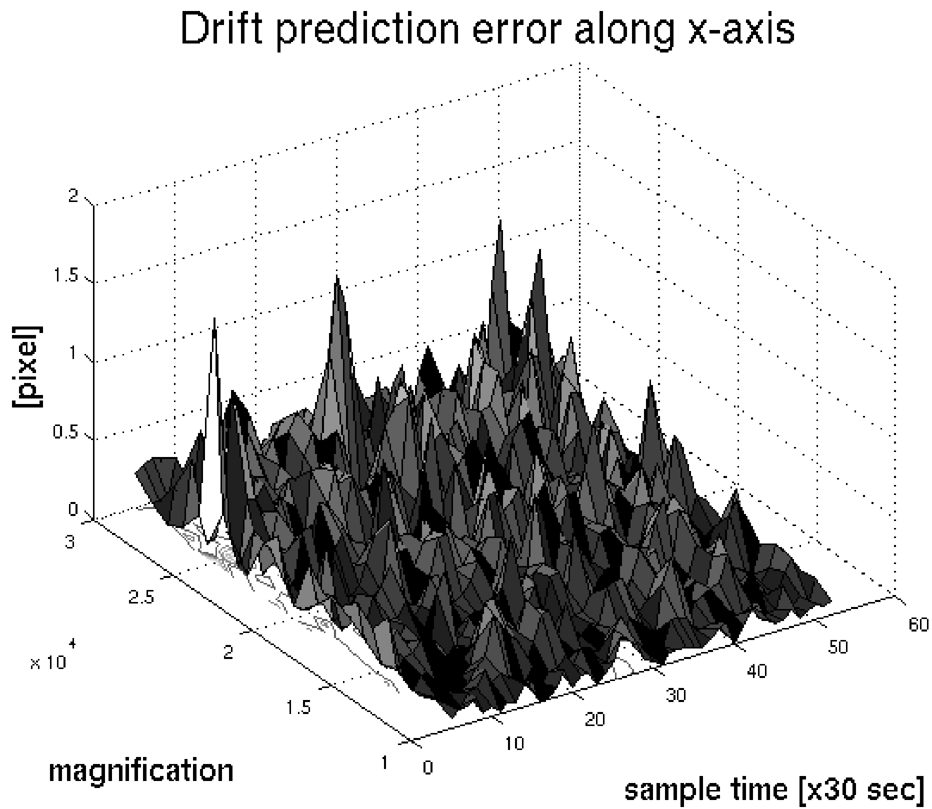

Figure 8: Tungsten SEM: the absolute error of drift with respect to time and magnification along x-axis.

hal-00799099, version 1 - 12 Mar 2013

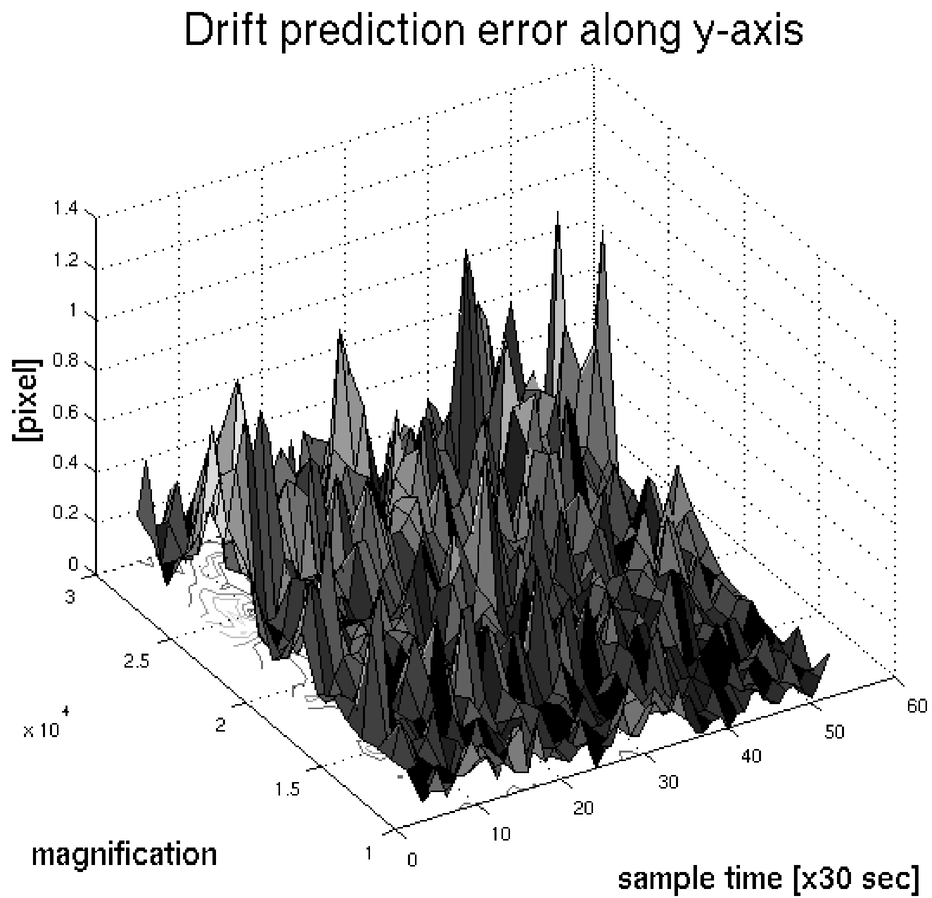

Figure 9: Tungsten SEM: the absolute error of drift with respect to time and magnification along y-axis.

hal-00799099, version 1 - 12 Mar 2013

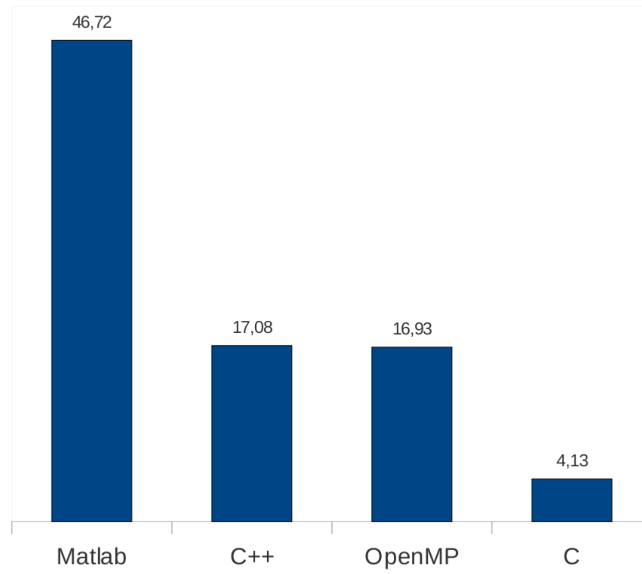

Figure 10: Tungsten SEM: the execution speed (in ms) of the correction for four implementations.

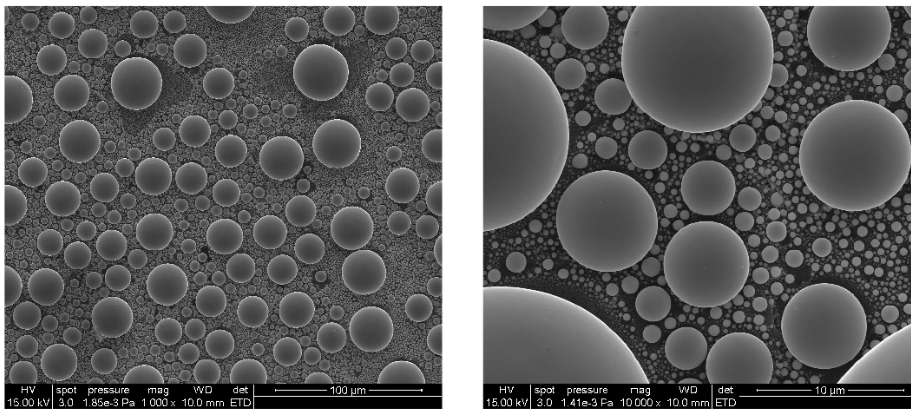

Figure 11: FE SEM: images of the tin-on-carbon calibration specimen at $1K\times$ (left) and $10K\times$ (right).

hal-00799099, version 1 - 12 Mar 2013

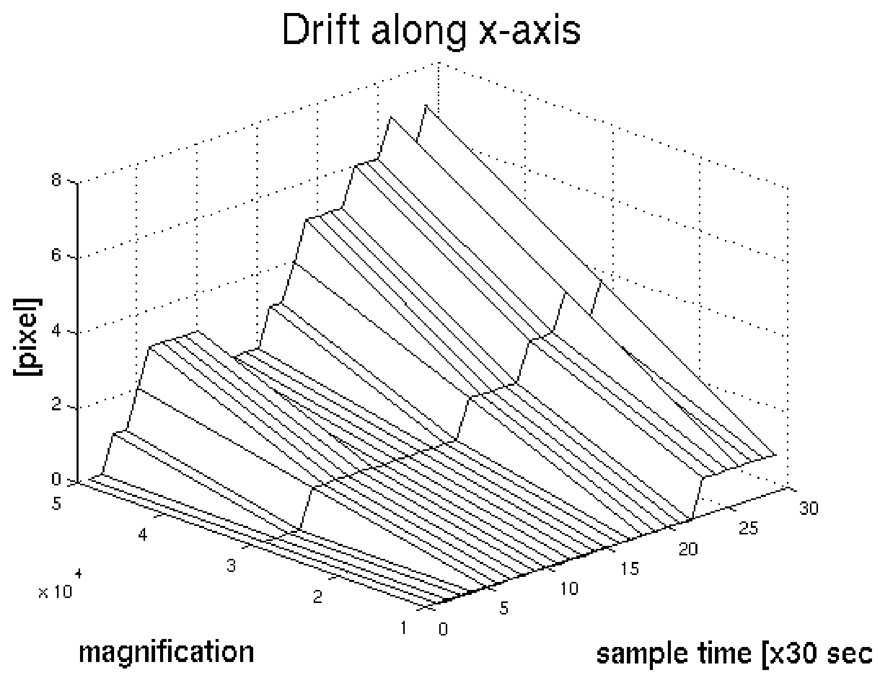

Figure 12: FE SEM: the drift with respect to time and magnification along x-axis.

hal-00799099, version 1 - 12 Mar 2013

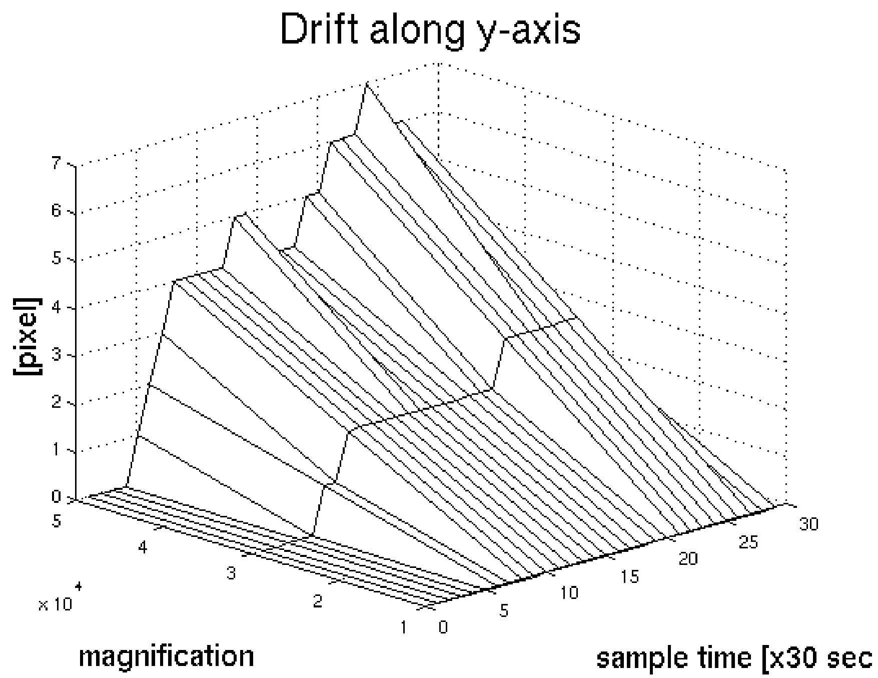

Figure 13: FE SEM: the drift with respect to time and magnification along y-axis.